Review article

Rotational velocity for oblique structures (Boltaña anticline, Southern Pyrenees)

Tania Mochales [a,*], Antonio M. Casas [b], Emilio L. Pueyo [a], Antonio Barnolas [c]

[a] Instituto Geológico y Minero de España, Oficina de Proyectos de Zaragoza, c/Manuel Lasala 44, 50006 Zaragoza, Spain
[b] Departamento de Ciencias de la Tierra, Universidad de Zaragoza, c/Pedro Cerbuna 12, 50009 Zaragoza, Spain
[c] Instituto Geológico y Minero de España, c/Rios Rosas 23, 28003 Madrid, Spain

A B S T R A C T

Despite the large amount of paleomagnetic and structural studies on fold and thrust belts, many key questions about rotational kinematics remain unsolved (pace of rotation, subsequent accommodation of the hanging wall, etc.). Excellent exposure conditions and syntectonic sedimentation related to the growth of oblique structures in the Southern Pyrenees allow an accurate investigation that sheds light on the rotational kinematics of thrust systems. Fifty-nine paleomagnetic sites (819 specimens) are homogeneously distributed in both limbs along the marine and continental sedimentary sequences contemporary with the uplift of the Boltaña anticline and its post-folding evolution. They indicate a clockwise rotation of about 52° during Ypresian to Priabonian times. Primary, stable (350°-580 °C), pre-folding magnetization in the Eocene rocks is attested by a positive fold test and the antipodality proof, with magnetite and iron sulphide traces as magnetic carriers. Rotation velocity fits a logarithmic model and shows a low rate during the Ilerdian-Middle Lutetian interval (ca. 1°/m.y.) and much higher (up to 10°/m.y.) in the Late Lutetian-Priabonian interval. Most of the clockwise rotation of the Boltaña anticline can therefore be constrained within the 42–35 M.a. interval (partially post-folding), indicating a period of strong differential displacement in the southern Pyrenean Zone, probably related to the emplacement of the underlying External Sierras thrust sheets (Tozal-Alcanadre).

© 2011 Elsevier Ltd. All rights reserved.

1. Introduction

During the past decades, paleomagnetic data revealed that orogenic building is usually associated with significant rotations around vertical axes (Allerton, 1998; Weil and Sussman, 2004). Paleomagnetic studies have the potential to identify rotations, not previously detected by structural techniques, providing absolute magnitude and sense of the rotation. Many studies, carried out in most orogenic belts, have allowed for previously unsuspected vertical axis rotations (VAR) to be inferred, as suggested by early works (synthesized in McCaig and McClelland, 1992), and more recent studies (Sussman et al., 2004; Arriagada et al., 2008; Weil et al., 2010, among others).

Once the existence of vertical axis rotation has been defined, determination of rotation velocities is a necessary step to define the kinematics of a particular thrust. Full understanding of rotational and traslational kinematics can turn into a real 4D comprehension of thrust systems. So far, only a few works have addressed the

rotational kinematics issue (Speranza et al., 1999; Pueyo et al., 2002; Mattei et al., 2004).

The structure of the Pyrenean range is characterized by a fold-thrust system with a WNW-ESE main trend. The southern Pyrenean Zone displays remarkable interference patterns between the main trend (in the frontal thrusts of the External, Marginal and Internal Sierras) and oblique folds. The Pico del Águila, Balzes (in the External Sierras), and Boltaña, Añisclo and Mediano (in the South Pyrenean Central Unit, SPCU, Fig. 1a) are the main N–S anticlines, progressively developed from E to W during Eocene times (Puigdefàbregas, 1975; Millán et al., 2000). Paleomagnetic data indicate that the origin of these oblique structures is secondary and related to important clockwise rotations (Dinarès, 1992; Parés and Dinarès, 1993; Pueyo, 2000; Fernández et al., 2004; Oms et al., 2006; Soto et al., 2006; Oliva and Pueyo, 2007; Rodríguez-Pintó et al., 2008).. The focus of this study lies in the particular configuration of the Boltaña anticline and its strongly oblique trend with respect to the Pyrenean tectonic grain (Fig. 1a).

In this paper we emphasize the use of paleomagnetism as the primary tool for determining the magnitude and chronology of VARs, we show a numerical model explaining the thrust rotation kinematics and we will propose a new model for the emplacement of the Boltaña anticline. Previous work (Fernández-Bellón, 2004)

* Corresponding author. Tel.: +34 976555153; fax: +34 976553358.
E-mail addresses: taniamochales@gmail.com, tania@unizar.es (T. Mochales), acasas@unizar.es (A.M. Casas), unaim@igme.es (E.L. Pueyo), a.barnolas@igme.es (A. Barnolas).
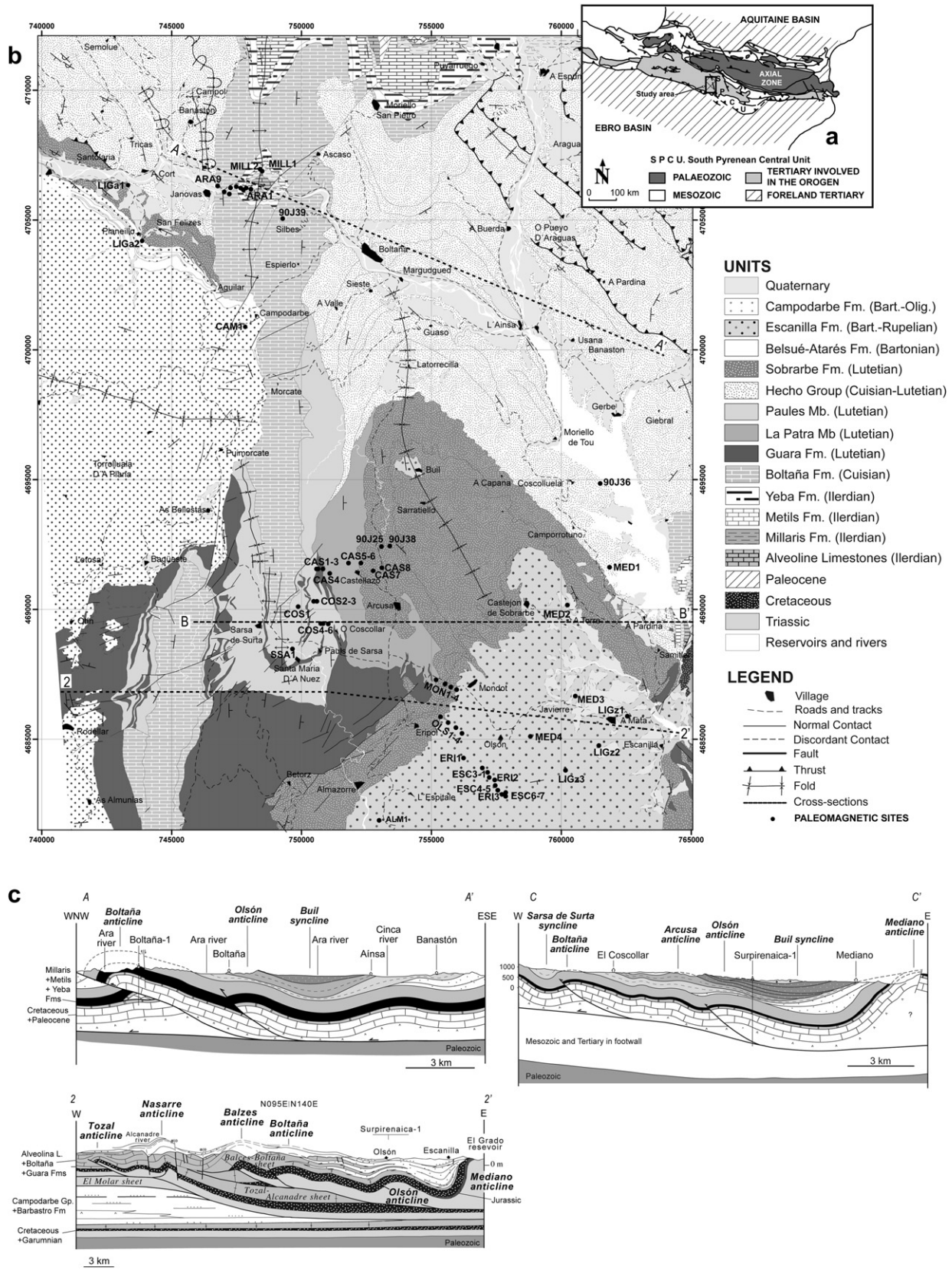
Fig. 1. a) The South Pyrenean foreland basin with the study area. b) Geological setting of the studied area (modified from Barnolas et al. in press-a, in press-b). Black points represent the sites sampled for this study (ARA, MILL, SSA, COS, CAS, MON, OLS, ESC), those reprocessed from Bentham (1992) (MED, LIGz, ERI, ALM) and individual sites from other authors: 90J25, 36, 38 39 from Dinarès (1992) and Parés and Dinarès (1993); LIGa and CAM from Pueyo (2000). Unit: Fm, Mb: Formation, Member. c) Cross-sections of the Boltaña anticline and Buil syncline (modified from Soto and Casas, 2001).

Table 1

Paleomagnetic data. New and previous individual sites presented in this work and data reprocessed data from Bentham (1992), Mochales et al. (2011), Pueyo (2000) and Parés and Dinarès (1993). Description: # number of site; Site label; Polarity; Stratigraphic length of the site; Age and Age error in M.a.; Chron; n/N: specimens considered and measured; Z: Zone; X and Y: UTM coordinates in datum ED50; Bedding data in right-hand rule; Paleomagnetic data *in situ* (Dec, Inc, α_{95} and kappa); Paleomagnetic data restored (Dec', Inc', α_{95}' and kappa'); Source in literature; Unit: Gp, Fm, Mb: Group, Formation, Member.

#	Site	Polarity	Site (m)	Age (M.y.)	Age error	Chron	n/N	Z	X	Y	Strike	Dip	DD	Dec	Inc	α_{95}	kappa	Dec'	Inc'	α_{95}'	kappa'	Source	Unit
1	ARA1	R	54.0	56.411	0.90	C24R	11/11	31T	254791	4706181	183	29	W	225	−35	12.7	17.1	200	−50	11.7	20.0	Mochales et al., 2011	Alveolina limestone
2	MILL1	R	45.0	56.062	0.90	C24R	14/15	31T	255245	4706873	193	6	W	240	−50	8.2	26.4	235	−54	8.4	24.9	Mochales et al., 2011	MillarisFm
3	MILL2	R	48.5	55.727	0.90	C24R	15/15	31T	255192	4706943	190	6	W	236	−37	7.9	28.3	231	−43	8.0	27.9	Mochales et al., 2011	MillarisFm
4	ARA2	R	60.5	55.513	0.90	C24R	16/15	31T	254554	4706256	183	29	W	226	−29	10.4	15.5	209	−53	9.5	16.1	Mochales et al., 2011	Metils Fm
5	ARA3	R	32.5	55.180	0.90	C24R	11/11	31T	254464	4706224	182	50	W	249	−9	10.7	21.1	230	−52	13.6	13.4	Mochales et al., 2011	Yeba Fm
6	ARA4	N + R	88.0	54.764	0.90	C24R	10/12	31T	254394	4706252	189	54	W	243	3	24.4	5.4	39	32	28.0	4.9	Mochales et al., 2011	Yeba Fm
7	ARA5	R	124.0	53.313	0.57	C24N.1r	12/13	31T	254216	4706317	184	63	W	67	−7	13.7	12.1	52	46	14.6	10.7	Mochales et al., 2011	Lw Boltaña Mb
8	ARA7	R + N	104.5	52.571	0.37	trC24n.1n/C23R	8/11	31T	253975	4706280	184	64	W	245	2	24.7	6.8	227	−52	19.8	10.0	Mochales et al., 2011	Lw Boltaña Mb
9	ARA6	R	97.0	52.565	0.37	C23R	14/14	31T	253910	4706069	188	72	W	252	22	8.3	25.7	246	−43	8.2	26.2	Mochales et al., 2011	Lw Boltaña Mb
10	ARA8	R	85.0	52.074	0.37	C23R	5/8	31T	253750	4706135	186	68	W	249	13	13.7	40.4	226	−50	15.0	33.6	Mochales et al., 2011	Upp Boltaña Mb
11	ARA9	R	85.0	50.241	0.65	C22R	4/6	31T	253519	4706413	187	82	W	229	33	35.9	19.3	226	−35	18.9	65.4	Mochales et al., 2011	Upp Boltaña Mb
12	SSA1	R	24.5	48.384	0.68	C21R	6/7	31T	254974	4688452	56	16	W	210	−55	8.4	77.4	232	−59	10.5	50.1	Mochales et al., 2011	Paules Mb
13	COS1	R + N	75.0	47.436	0.68	C21R	12/14	31T	255470	4690014	358	18	E	197	−67	7.0	43.6	223	−58	7.1	41.9	Mochales et al., 2011	Paules Mb
14	COS2	R + N	42.0	45.226	1.29	C20R	13/15	31T	256062	4690160	350	27	E	184	−63	6.5	45.4	221	−48	7.3	36.1	Mochales et al., 2011	Paules Mb
15	COS3	R	30.0	44.889	1.29	C20R	14/15	31T	256184	4690146	350	25	E	199	−63	5.4	59.7	225	−46	6.2	45.6	Mochales et al., 2011	Paules Mb
16	COS4	R	48.0	44.734	1.29	C20R	11/11	31T	256266	4689306	359	20	E	203	−64	4.3	124.0	224	−50	7.2	45.7	Mochales et al., 2011	Paules Mb
17	COS5	R	42.0	44.308	1.29	C20R	11/11	31T	256376	4689286	359	27	E	199	−67	12.0	17.0	226	−50	12.2	16.6	Mochales et al., 2011	Paules Mb
18	COS6	R	42.0	43.900	1.29	C20R	12/12	31T	256562	4689281	356	26	E	188	−69	7.7	35.7	226	−55	6.5	50.3	Mochales et al., 2011	Paules Mb
19	CAS1	R	45.0	43.346	1.29	C20R	9/10	31T	256294	4691407	350	23	E	218	−73	7.1	59.5	240	−52	7.0	61.3	Mochales et al., 2011	La Patra Mb
20	CAS2	R	35.0	42.982	1.29	C20R	10/10	31T	256321	4691421	352	26	E	210	−60	20.4	7.3	227	−45	21.0	7.0	Mochales et al., 2011	La Patra Mb
21	CAS3	N + R	65.0	42.620	0.59	C20N	6/7	31T	256494	4691358	5	27	E	3	63	22.0	12.3	41	53	19.8	14.8	Mochales et al., 2011	La Patra Mb
22	CAS4	N + R	72.0	42.369	0.59	C20N	12/13	31T	256746	4691181	356	20	E	45	60	18.9	6.8	57	50	16.1	9.0	Mochales et al., 2011	La Patra Mb
23	CAS5	N + 1R	42.0	42.115	0.59	C20N	8/10	31T	257491	4691559	4	22	E	340	56	13.8	19.5	15	58	12.7	22.7	Mochales et al., 2011	La Patra Mb
24	CAS6	N	139.0	41.777	0.59	C20N	11/12	31T	257975	4691523	357	24	E	18	59	10.9	20.4	44	46	11.1	19.8	Mochales et al., 2011	La Patra Mb
25	MON1	R + N	47.5	41.619	0.59	C20N	9/11	31T	260535	4686825	8	23	E	195	−52	12.0	21.7	218	−41	12.3	20.7	Mochales et al., 2011	Sobrarbe Fm
26	CAS7	R	105.0	41.377	0.46	C19R	10/12	31T	258412	4691197	354	21	E	207	−56	8.1	40.9	224	−41	8.3	38.4	Mochales et al., 2011	Sobrarbe Fm
27	MON2	R + N	71.0	41.367	0.46	C19R	10/12	31T	260888	4686646	10	22	E	180	−59	7.5	46.8	213	−55	6.4	64.0	Mochales et al., 2011	Sobrarbe Fm
28	MON3	R	39.0	41.193	0.46	C19R	11/11	31T	261090	4686522	10	23	E	193	−51	9.5	26.7	218	−45	9.3	27.5	Mochales et al., 2011	Sobrarbe Fm
29	CAS8	R	11.0	41.152	0.46	C19R	3/4	31T	258754	4691296	352	22	E	205	−55	20.5	55.8	224	−41	20.6	55.4	Mochales et al., 2011	Sobrarbe Fm
30	OLS1	R + N	122.0	41.084	0.46	C19R	9/10	31T	260618	4685394	34	25	E	215	−36	16.0	12.7	233	−32	14.8	14.6	Mochales et al., 2011	Sobrarbe Fm
31	MON4	N + R	75.5	40.993	0.46	C19R	12/12	31T	261307	4686392	23	17	E	16	49	19.0	7.4	33	49	18.0	8.2	Mochales et al., 2011	Sobrarbe Fm
32	OLS2	R + N	93.5	40.703	0.46	C19R	8/12	31T	260898	4685156	36	21	E	215	−32	13.4	20.5	218	−24	14.7	17.4	Mochales et al., 2011	Escanilla Fm
33	OLS3	R + N	80.5	40.439	0.49	C18R	9/11	31T	261182	4684942	45	16	E	208	−16	24.4	6.1	206	−21	24.4	6.1	Mochales et al., 2011	Escanilla Fm
34	OLS4	R + 1N	56.5	39.777	0.49	C18R	10/11	31T	261394	4684706	91	16	E	29	36	13.2	16.0	214	−41	12.8	17.0	Mochales et al., 2011	Escanilla Fm
35	ERI1	N + R	345	38.548	0.47	C18N.1n	13/18	30T	756252	4684372	130	14	S					36	55	15.6	8.7	Bentham, 1992	Escanilla Fm
36	ESC3	N	4	37.451	0.10	≈C17N.2n	15/15	31T	262072	4683329	80	10	S	31	27	13.4	9.7	35	34	13.4	9.7	This work	Escanilla Fm
37	ESC2	N	10	37.129	0.36	≈C17N.1n	10/14	31T	262256	4683133	68	13	SE	27	45	14.0	14.2	39	52	14.0	14.2	This work	Escanilla Fm
38	ESC1	N	17	36.814	0.29	≈C16N.2n	11/15	31T	262320	4682955	65	15	SE	18	50	8.9	30.0	35	60	8.9	30.0	This work	Escanilla Fm
39	ERI2	N + 1R	279	36.401	0.36	≈C17N.1n	13/14	30T	757446	4683539	151	11	W					27	48	9.0	23.9	Bentham, 1992	Escanilla Fm
40	ESC4	N	6	35.902	0.29	≈16N.2n	11/13	31T	262532	4682604	95	10	S	26	17	9.7	25.5	27	26	9.7	25.5	This work	Escanilla Fm
41	ESC5	R	5	35.707	0.07	C16N.1r	7/11	31T	262605	4682420	85	16	S	195	21	12.5	28.5	198	−36	12.5	28.5	This work	Escanilla Fm
42	ERI3	N + R	200	35.284	0.18	C15R	13/14	30T	757824	4682909	155	10	W					21	47	13.0	12.1	Bentham, 1992	Escanilla Fm
43	ESC6	R	2	35.067	0.31	≈C15	10/10	31T	262776	4682247	85	16	S	180	−31	7.3	49.3	181	−47	7.3	49.3	This work	Escanilla Fm
44	ESC7	N + 1R	5	35.043	0.13	C15N	13/13	31T	262872	4682316	83	3	S	1	44	4.1	110.6	2	47	4.1	110.6	This work	Escanilla Fm
45	ALM1	R + N	275	38.870	0.50	trC18R.1r/18N.1n	11/13	30T	753214	4681982	128	90	S					26	38	15.8	10.2	Bentham, 1992	Escanilla Fm
46	MED1	N + R	549	41.58	0.59	C20N	14/15	30T	761828	4691753	247	26	N					17	52	14.3	9.4	Bentham, 1992	Hecho Gp
47	MED2	N	425	40.55	0.12	C19n	14/14	30T	760233	4690298	241	18	N					27	59	9.0	22.1	Bentham, 1992	Sobrarbe/Escanilla Fm
48	MED3	N + R	296	36.980	0.21	trC17N.3n/17N.2n	15/15	30T	760540	4686788	230.6	11.8	NW					32	33	14.3	8.7	Bentham, 1992	Escanilla Fm

#	Site	Pol		Age		N	Chron	Dec	Inc		Dec	Inc	a95		Dec	Inc	a95		Reference	Formation
49	MED4	N + R	359	37.240	0.42	11/14	trC17N.1r/17N.1n	183	6	W					27	46	10.2	23	Bentham, 1992	Escanilla Fm
50	LIGz1	R + N	259	38.660	1.20	11/14	trC18R/18N.1n	227	12	N					22	42	17.9	8.2	Bentham, 1992	Escanilla Fm
51	LIGz2	N + 1R	316	36.480	0.42	11/14	trC17N.1r/17N.1n	230	9	N					24	51	12.1	16.6	Bentham, 1992	Escanilla Fm
52	LIGz3	N + R	223	35.010	0.39	14/14	trC16N.1n/15N	165	11	W					22	47	14.4	9.2	Bentham, 1992	Escanilla Fm
53	LIGa1	R + N		40.670	0.56	10/10	trC19r/19n	146	68	W	226	29	22	5	222	−38	22	5	Pueyo, 2000	Sobrarbe Fm
54	LIGa2	R	5	42.27	0.59	10/10	C20N	154	54	W	230	18	20	6	225	−34	20	6	Pueyo, 2000	Belsué-Atarés Fm
55	CAM1	N	5	37.99	0.72	6/7	trC18N.2n/18N.1n	150	20	W	5	37	21	9	346	45	21	9	Pueyo, 2000	Campodarbe Gp
56	90J25	N		41.06	0.46	4/4	C19R	155	7	SW	45	42	38.8	6.6	42	49	38.8	6.6	Parés and Dinarès, 1993	Sobrarbe Fm
57	90J36	N + R		42.6	0.6	5/5	C20n	143	17	SW	48	38	8.8	76.3	46	55	9.3	69	Parés and Dinarès, 1993	Hecho Gp
58	90J38	R		41.370	0.46	2/2	C19R	351	40	E	161	−66	23	120.5	224	−48	23	120.4	Parés and Dinarès, 1993	Sobrarbe Fm
59	90J39	R		50.320	0.65	5/7	C22R	17	15	SW	233	−57	14.1	19.2	247	−47	14.1	19.3	Parés and Dinarès, 1993	Boltaña Fm

approached to the rotation in the oblique structures of the Ainsa Basin by means of scattered paleomagnetic sites. In this work, we provide a dense, homogenous and age-controlled dataset for the determination of rotation that allows for establishing a rotational velocity model and a more detailed kinematic hypothesis.

With this aim, we introduce new paleomagnetic data, we revisit previous magnetostratigraphic works and we consider other previous paleomagnetic sites in the area. From this unusually large dataset and taking advantage of the recently proposed chronological frame for the Ainsa Basin (Mochales et al., 2011), 59 paleomagnetic sites evenly distributed along the stratigraphic pile (Lower to Upper Eocene) can be precisely dated, with the final objective of understanding the rotational kinematics of this structure.

2. Geological setting

The Pyrenean range formed during the convergence between the Iberian and European plates, partially inverting inherited extensional basins (Roure et al., 1989; Choukroune and ECORS team, 1989; Muñoz, 1992; Teixell, 1998; Vergés and García Senz, 2001; Martínez-Peña and Casas-Sainz, 2003; Soto et al., 2003; McClay et al., 2004). Several tectonic pulses taking place from Late Cretaceous to Miocene times ended up shaping a WNW-ESE range. The South Pyrenean Central Unit (SPCU) constitutes a salient including three main thrust units sequentially emplaced from north to south: Bòixols, Montsec and Marginal Sierras (Séguret, 1972; Pocoví, 1978; Vergés and Muñoz, 1990; Muñoz, 1992). These cover thrust sheets are composed of Mesozoic and Paleogene sediments detached from the Palaeozoic substratum on Triassic evaporite layers (Séguret, 1972; Cámara and Klimowitz, 1985; Muñoz, 1992; Anastasio, 1992). The Mesozoic cover of the SPCU overthrusts the Tertiary deposits of the Ebro Basin, which are found in the footwall of the Pyrenean thrusts (Pocoví, 1978; Vergés and Muñoz, 1990; Muñoz, 1992; Teixell and Muñoz, 2000).

The Boltaña anticline constitutes the boundary between the Tremp-Graus and Jaca Basins. The Ainsa Basin corresponds to the westernmost part of the piggyback Tremp-Graus Basin, which was transported in the hanging wall of the Montsec thrust (Garrido-Megías, 1973; Mutti et al., 1988). The Ainsa Basin was filled with Paleocene and Eocene deposits, concomitant to the major compressional episode (Lutetian−Bartonian) in the Southern Pyrenees.

2.1. Stratigraphy

The older rocks cropping out in the Boltaña anticline are Lower Eocene limestones (Alveoline limestones, less than 75 m thick). Marls and marly limestones (Millaris and Metils Fms, 125 m thick, Van Lunsen, 1970), and a deltaic sequence (Yeba Fm, 200 m thick, Van Lunsen, 1970) overlie the previous unit. The Boltaña Fm (650 m thick, Barnolas et al., 1991) represents the upper part of the Ypresian deposits, with large outcrops in the Boltaña anticline (Fig. 1a). The lower part of the Boltaña Fm presents mixed platform features (siliciclastic and calcareous), and its upper part is calcareous. Marly layers of distal ramp and carbonate slope facies, including debris sheets of olistoliths sourced in the carbonate platform (Barnolas et al., 1991) overlie the Boltaña Fm. The transition from shallow platform to carbonate slope facies represents a drowning unconformity, implying a forelandward migration of the carbonate platform (Barnolas and Teixell, 1994). Lutetian carbonate slope facies crop out in both limbs of the Boltaña anticline, although in this study they were only surveyed in its eastern limb. The slope facies are included in the San Vicente Fm (Van Lunsen, 1970), where the Paules and La Patra Members (De Federico, 1981) can be

distinguished. Both units are composed of marls and nodular marly limestones ($\approx$800 m). The Paules Member shows a retrogradational pattern with erosive slump scars; La Patra Member is progradational, with thick sequences of carbonate debris sheets including olistoliths (Barnolas et al., 1991). The deltaic strata of the Sobrarbe Fm (De Federico, 1981) overlie the previous succession, prograding towards the northwest in the Buil syncline and the western limb of the Boltaña anticline ($\approx$250 m). Red beds (Escanilla Fm, 1000 m thick, Garrido-Megías, 1968), Bartonian to Lower Oligocene in age, overlie the Sobrarbe Fm. They are linked to braided fluvial channel deposition (Bentham, 1992; Bentham and Burbank, 1996). Finally, the Oligo-Miocene Graus conglomerates (Sariñena Fm, Quirantes, 1978) lie unconformably on the Eocene series. They are related to Ebro Basin alluvial fans and grade laterally into sandstones and siltstones in the foreland (Luzón, 2005).

2.2. Structure

The Boltaña anticline is a west-verging, N–S trending (N004E), 25 km long cylindrical fold (Puigdefàbregas, 1975; Cámara and Klimowitz, 1985; Martínez Peña, 1991; Holl and Anastasio, 1995; Millán, 1996; Soto et al., 2003; Fernández-Bellón, 2004). It shows non-significant plunge, except for its southern part where a gentle fold closure is observed. Its eastern flank shows shallower dips (20–30°) than its western flank (70–80°). The Boltaña anticline is interpreted to have formed in relation to a blind thrust with westwards movement (Cámara and Klimowitz, 1985; Farrell et al., 1987; Mutti et al., 1988; Martínez Peña, 1991; Holl and Anastasio, 1995; Millán, 1996; Muñoz et al., 1998; Soto and Casas, 2001; Fernández et al., 2004). The thrust-anticline system (Balzes-Boltaña sheet; Millán, 1996) is located in the hanging wall of the younger Alcanadre-Tozal thrust sheet located in the External Sierras front to the South of the studied area (Millán, 1996). The Triassic evaporites form the detachment level to the south Pyrenean thrust system. Pre-tectonic rocks overlying the evaporitic level are mainly of Cretaceous-Ypresian age (as deduced from the Boltaña-1 well data; Lanaja, 1987). Cuisian units thin toward the south, defining a sedimentary wedge probably related to tectonic subsidence associated with thrust sheet emplacement in the Axial Zone (Fonnesu, 1984; Puigdefàbregas et al., 1986; Soto and Casas, 2001; Mochales et al., 2010). The Lower Lutetian is the first syntectonic sequence related to the Boltaña anticline, as evidenced by i) the onlap of the Hecho Group turbidites on the eastern limb of the Boltaña anticline (Puigdefàbregas, 1975; Remacha and Fernández, 2003), ii) thickness changes in the stratigraphic pile (Soto and Casas, 2001), iii) unstable slope marls at the bottom of the San Vicente Fm (Barnolas and Gil-Peña, 2001; Mochales et al., 2011) and iv) kinematics inferred from magnetic fabrics (Mochales et al., 2010). Large-scale basinal response to tectonic activity (flexure and deepening of the basin) is recorded in Early Lutetian stages. The growth of the Boltaña and Añisclo anticlines was linked to the Larra thrust system, which developed from mid-late Lutetian to Bartonian times (De Federico, 1981; Montes, 1992; Teixell, 1992; 1996). Oligocene-Miocene molasse sediments postdate the developing of the oblique structures of the Ainsa Basin (Luzón, 2005).

3. Paleomagnetic data

3.1. Sampling and laboratory procedures

Fifty-nine sites were drilled or reprocessed in different structural positions and rock types, covering pre- and syntectonic sequences involved in the Boltaña anticline and Buil syncline (Fig. 1b,c, Table 1), totalling 566 (used) from 1253 (total) specimens.

From this set, we re-processed the results obtained in magnetostratigraphic studies (Ara, Bal Ferrera, Coscollar and Mondot sections by Mochales et al. (2011), and Eripol section by Bentham (1992)), gathering them into 37 evenly distributed VAR sites. Bentham's (1992) data in the Escanilla Fm (Almazorre; Ligüerre and Mediano sections) were reprocessed, defining 8 reliable sites (15 specimens in average). VAR sites derived from previous magnetostratigraphic studies (Mochales et al., 2011) were established according to the following criteria: 1) Geographic proximity of samples; 2) Samples within the same magnetostratigraphic section and stratigraphic unit; 3) Samples belonging to the same Chron; 4) A minimum of 10 samples per site (except for 5 sites, Table 1); 5) Only high quality directions (at the specimen scale) from the magnetostratigraphy were used to obtain VAR values (see below). Additional VAR magnitudes that come from 7 previous standard sites (90J sites by Dinarès (1992); Parés and Dinarès (1993); LIG1&2 and CAM1 sites by Pueyo (2000)) have also been considered. Finally, 7 new sites were drilled in the Escanilla Fm (ESC sites in this work). The chronological background established by means of magnetostratigraphy (Mochales et al., 2011), allows for the accurate dating of VAR changes through Eocene times.

Samples were extracted using a petrol-powered drill cooled by water. All the cores were geo-referenced in situ with a GPS and oriented with a magnetic compass. Standard specimens (cylinders 21 × 25 mm Ø) were measured by means of 2G DC-SQUID magnetometers, placed into shielded rooms laboratories (Bethlehem, USA and Rome, Italy), under Helmholtz coils (Burgos, Spain and Tübingen, Germany) and without shielding (Barcelona, Spain). The background noise in all of them was below 5×10^{-6} A/m. MMTD60 ovens (Magnetic Measurement) were used in Burgos and Barcelona and TDS-1 ovens (Schonstedt) in Barcelona, Tübingen, Bethlehem and Rome laboratories. Demagnetization procedures changed depending on the rock type. At least one specimen per core was thermally demagnetized. Several sister samples were demagnetized by alternating field procedures, but thermal treatment revealed more efficiently Characteristic Remanent Magnetization (ChRM). Thermal demagnetization in limestones consisted of 16–19 steps, with increments in key intervals around 20°, up to 580 °C. In the case of marls, it included 12–20 steps, with the smallest increments of 20°, up to 600 °C. In detrital rocks, demagnetizations were performed with 20–25 steps, with key intervals of 5°, reaching 695 °C. Alternating field magnetization intervals followed arithmetic increments to 100 mT.

ChRM were classified according to three quality levels (Fig. 2). High quality ChRMs are unequivocal and data plotted on orthogonal demagnetisation graphs pointed straight to the origin. Intermediate quality ChRMs unambiguously allow polarity recognitions, although directions are less reliable and seem to be altered by sedimentary load and magnetic secondary overlapping. In the low quality ChRMs, some directional data could be extracted. However, they were not reliable (because of poor definition, anomalous inclinations or intensities), and consequently discarded. To gain reliability, only high quality ChRMs were used for VAR studies, and 45% (566 specimens) from the total analyzed samples (1253 specimens) were used. A fold test was performed by means of the superIAPD software (by T.H. Torsvik, 1986, based on McElhinny (1964) criteria. Antiparallelism was checked by Fisher's statistics (1953). The Geological Time Scale considered was Gradstein et al. (2004).

Magnetic carriers were deduced from rock magnetism analyses. MMPM Pulse-Magnetizer (Tübingen), ASC impulse magnetizer (Lehigh), 2G pulse magnetizer (Rome) and 2G cryogenic magnetometers were used to perform IRM coercivity spectrum analyses. Between 24 and 30 increasing fields up to 1.8 T were applied. About 90 samples were subjected to the Lowrie test (1990). Subsequently,
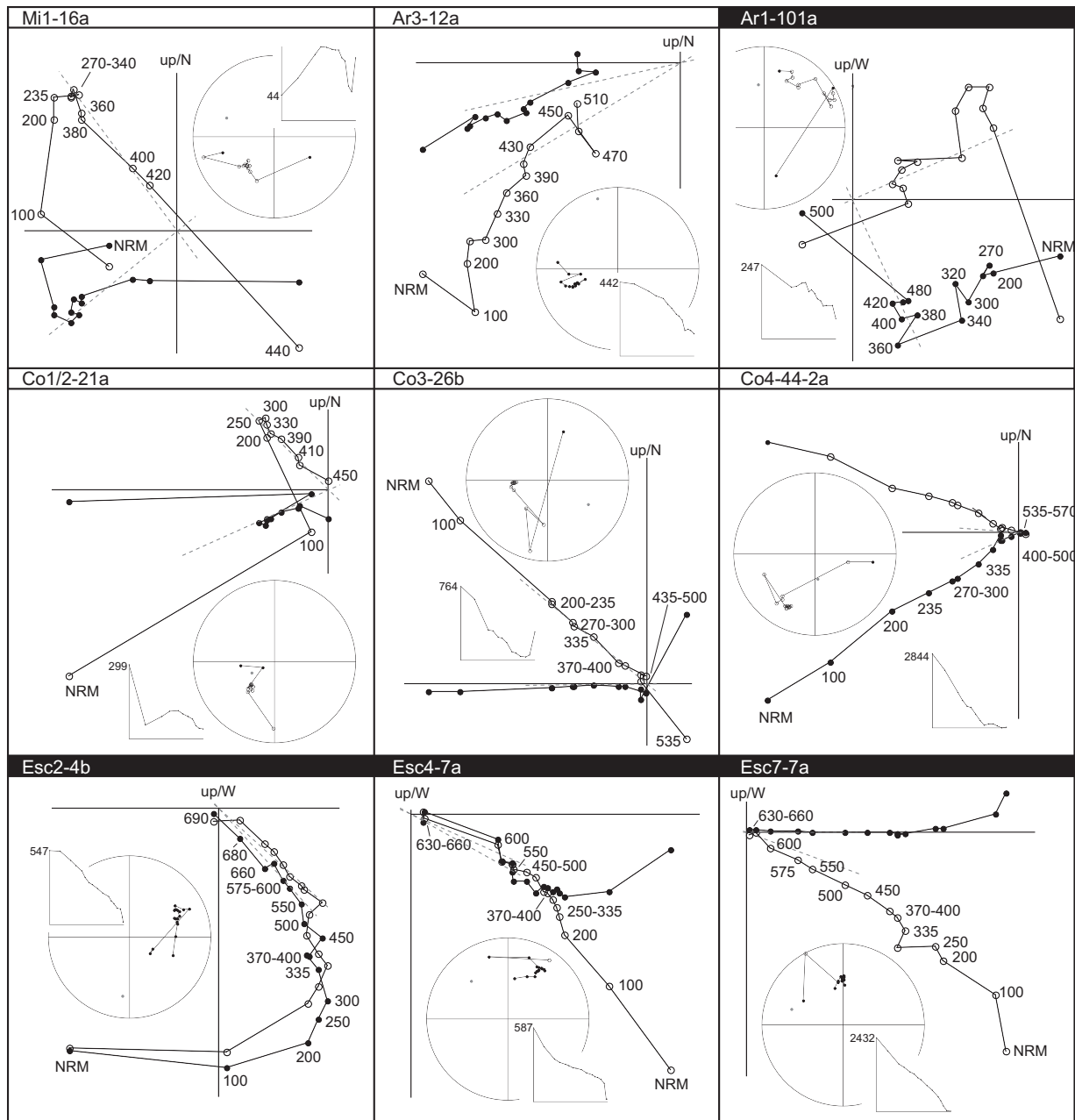
Fig. 2. Illustrative *in situ* Zijderveld diagrams of thermal demagnetization in several sites. MI and AR correspond to Ypresian rocks, CO to Lutetian and ESC to Bartonian-Priabonian. Stereoplots with intensity drops are shown. NRM is 10^{-6} A/m magnitude.

thermal stepwise demagnetization was carried out with 35°–50 °C increments, up to 600 °C. Through an AGFM 2900 (Princeton Measurements Corp.) Alternating Gradient Force magnetometer at Tübingen laboratory, 51 hysteresis loops were performed (Fig. 3).

4. Results

4.1. NRM components

Since different rock types were sampled, Natural Remanent Magnetization (NRM) and magnetic susceptibility are highly variable (Table 2). The ChRMs could be isolated in the 320–500 °C temperature interval in the Ypresian samples (from Alveoline limestones to Boltaña Fm), 350–580 °C in the Lutetian slope marls and deltaic facies (San Vicente and Sobrarbe Fms) and between 360

and 680 °C in the fluvial materials of the Escanilla Fm (Bartonian-Priabonian). Alternating field demagnetizations were less efficient than thermal cleaning. Thermal demagnetizations allowed recognizing a low-temperature component unblocking below 200 °C and AF analysis a low-field component below 10 mT. These components were discarded since they evidence a recent overprint.

Fifty-two site-mean paleomagnetic directions were calculated (Table 1) by means of Fisher (1953) statistics. All sites in marly units provide well-defined directions, with $\alpha_{95} < 9.5°$ (MILL1, MILL2, ARA2). Sites in limestones display relatively clustered directions (ARA1). Scattering in paleomagnetic vectors is observed for sandy facies (sites: ARA4, 7, 9). In the case of carbonate slope marls, clustering is observed in each site, with maximum α_{95} of 12.7, except for CAS2, 3, 4 where a turbiditic channel was sampled. The upper part of the Sobrarbe Fm, and the Escanilla Fm show slightly
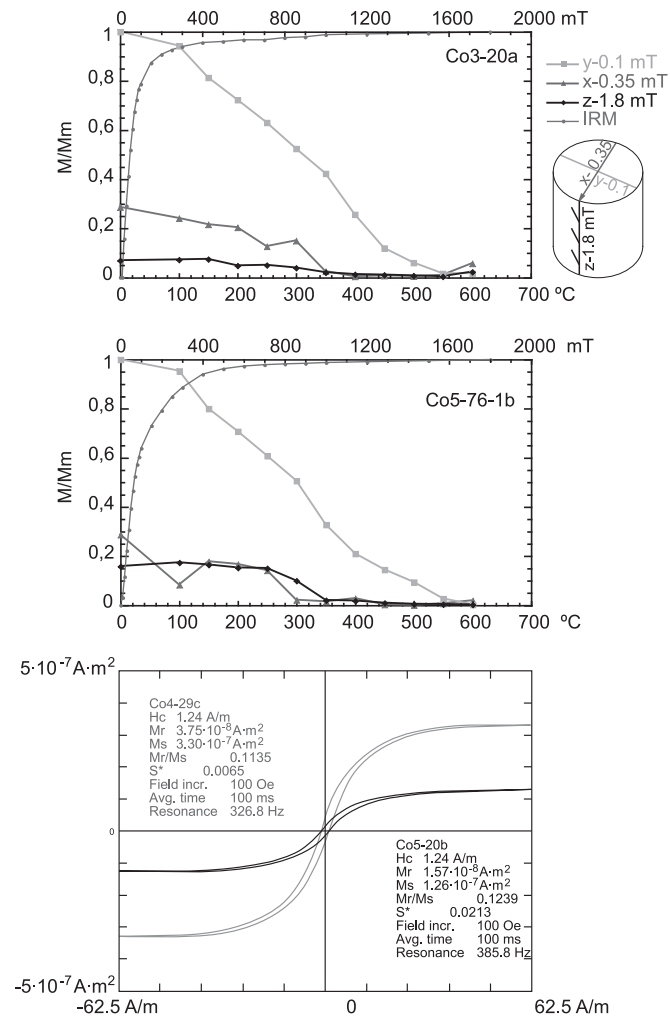
Fig. 3. Rock magnetism analyses. a and b) Lowrie test analysis (1990) and IRM acquisition curves of two specimens. Lower abscissa represent the Lowrie test (1990) temperatures, upper abscissa is the increasing field (mT) applied to IRM. In y-axis, normalized remanent magnetization. Decreasing magnetic fields were applied along z (1.8 mT), x (0.35 mT) and y axes (0.1 mT). c) Hysteresis loops, on the abscissa the magnetic field strength and in ordinates the magnetic moment. Hysteresis loops indicate low cohercity minerals as magnetite and iron sulphides.

higher α_{95} angles, especially CAS8 and OLS3 (Fig. 4). Re-processing Bentham's (1992) data offered better results grouped into stratigraphically homogeneous sets, showing acceptable α_{95} angles (Table 1). Therefore most sites ($\approx 70\%$) yielded reliable Characteristic Remanent Magnetization (ChRM) with α_{95} angles lower than

Table 2
Detailed NRM intensities (10^{-6} A/m) and bulk susceptibilities (10^{-6} S.I.) of the formations involved in the study.

Formation	Mean NRM (10^{-6} A/m)		Mean K ($\cdot 10^{-6}$ S.I.)	K standard error
Alveoline Lms.	446	55.4	16	7.4
Millaris Fm	140	38.9	90	18.6
Metils Fm	714	73.8	33	4.7
Yeba Fm	293	82.8	73	11.7
Boltaña Fm	192	16.9	61	6.9
Ascaso Mb	93	27.3	8	3.2
Paules Mb	102	7.2	20	2.5
La Patra Mb	356	46.9	57	9.6
Sobrarbe Fm	232	105.0	86	10.9
Escanilla Fm	1100	264.4	112	8.4

15° (both before and after bedding correction), except for 10 sites from the re-processed magnetostratigraphy (Bentham, 1992; Mochales et al., 2011) and five individual sites from other authors (Dinarès, 1992; Parés and Dinarès, 1993; Pueyo, 2000). The age of the sampled sites was tightly constrained based on new chronological information ((Bentham, 1992; Mochales et al., 2011) and five individual sites from other authors (Dinarès, 1992; Parés and Dinarès 1993; Pueyo, 2000). The age of the sampled sites was tightly constrained based on new chronological information (Mochales et al., 2011) (Table 1). Finally, we used the reference established by Taberner et al. (1999) for the Eocene in the South-eastern Pyrenean Basin (Dec: 004, Inc: 53, α_{95}: 4.6°, k: 9.6) to constraint the local VARs in the studied area.

4.2. Paleomagnetic stability

Site means were considered for the fold test. Sites are located on the western (ARA), and eastern (COS, CAS and MON) limbs of the Boltaña anticline. Only sites with $\alpha_{95} <10^\circ$ (*in situ*) were retained. The fold test, according to McElhinny (1964) statistics, confirms the pre-folding character of the ChRM component (Fig. 5a), according with evidence in the southernmost Pyrenean units (Pueyo, 2000; Larrasoaña, 2000; Larrasoaña et al., 2003). Due to the lack of internal deformation and the absence of restoration problems (Pueyo, 2010), the slight and non-significant synfolding character of the magnetization is probably due to an unimportant overlapping with younger components, as already pointed out in the Lutetian platform facies (Rodríguez-Pintó et al., 2010).

Statistics of the two magnetic polarities (site means) reveal pseudo-antipodal directions, considering the α_{95} angles (Fig. 5b): Normal: n = 7, Dec, Inc = 046, 47, α_{95} = 6.5, k = 86.6, R = 6.9307 and Reverse: n = 27, Dec, Inc = 225, −47, α_{95} = 3.2, k = 74.7, R = 26.6517. All this evidence based on all the sites sampled in this work (ARA, COS, CAS, MON, OLS and ESC) together with the pattern of reversals (Mochales et al., 2011) indicate the primary character of the magnetization.

4.3. Reliability of data

Datasets in paleomagnetism must respect some reliability criteria (Van der Voo, 1990) and should be carefully evaluated to guarantee the absence of the more common sources of error (Pueyo 2010): 1) non-existence of internal deformation (rigid body assumption), 2) a perfect laboratory isolation of components (absence of overlapping) and 3) correct restoration to the ancient reference system (not necessarily based on the bedding correction). Some overlapping of components has been observed, especially in Ilerdian (Ypresian) rocks. Therefore, aiming to avoid sites with noisy signal, a strict filtering was done at the site scale. From the vast dataset only samples with unambiguous ChRMs were selected for VAR interpretation. Sites with anomalous inclinations and high α_{95} angles ($>20^\circ$) were discarded, retaining 68% of the original sites in the dataset (Fig. 6a and Table 1).

5. Interpretation and discussion: vertical axis rotations in the Boltaña anticline

A considerable amount of studies have been carried out with the aim of clarifying the kinematics of oblique structures west of the SPCU. Nonetheless, several aspects are not solved so far. Existing studies indicate clockwise rotation values ranging from 25° to 85° (Dinarès, 1992; Parés and Dinarès, 1993; Bentham and Burbank, 1996; Pueyo, 2000; Fernández-Bellón, 2004; Oms et al., 2006). These authors point out a decrease of the rotation value eastwards, either due to synsedimentary rotation, or to deposition of
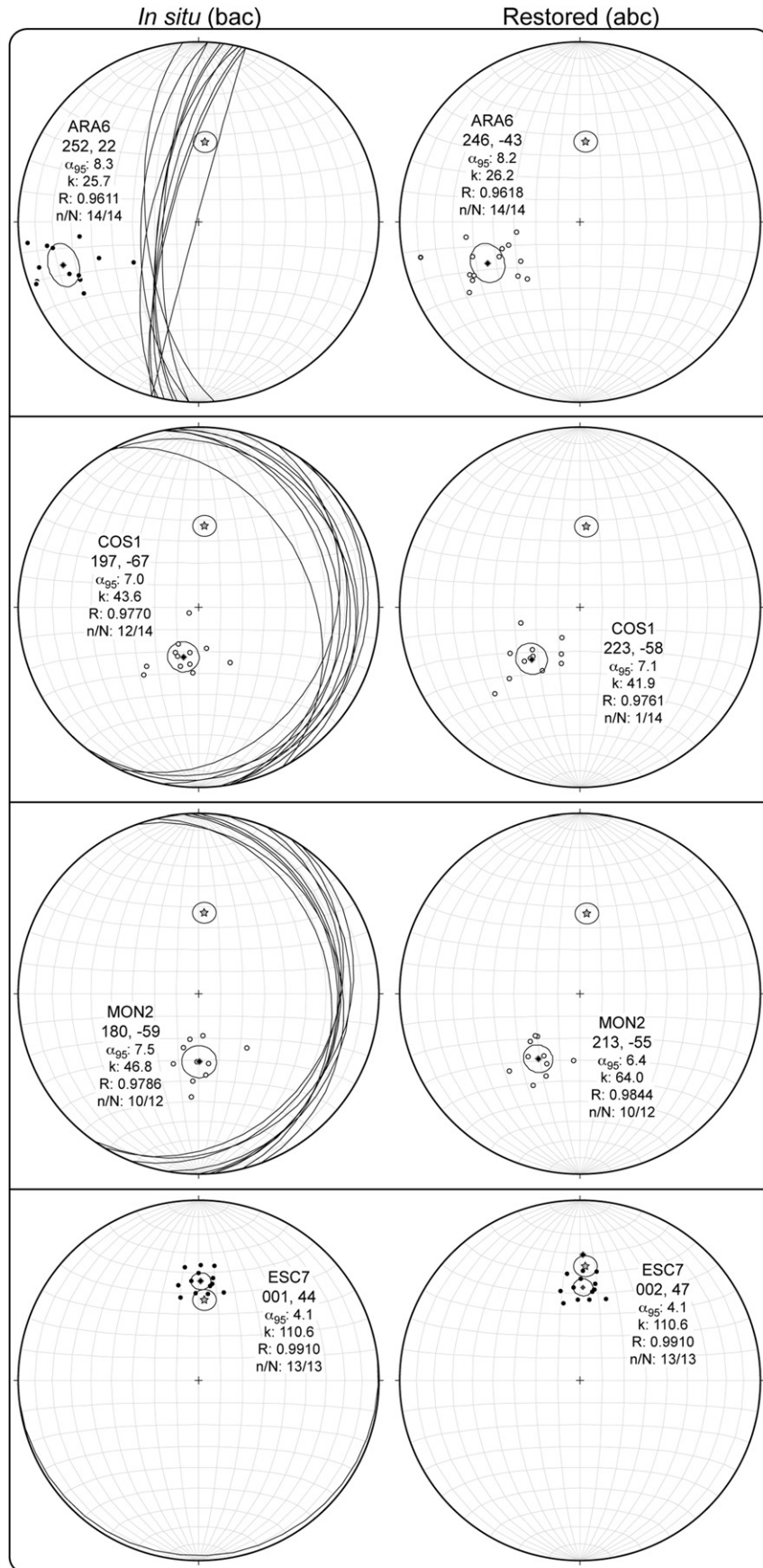
Fig. 4. Representative site means (equal area) with Dec, Inc, a$_{95}$, kappa, R and n/N sites details. Left column shows *in situ* vectors (bac) with bedding, whereas right column represents restored vectors (abc). Stars indicate the Eocene reference (Dec, Inc, a$_{95}$: 004, 55, 3) established by Taberner et al. (1999).
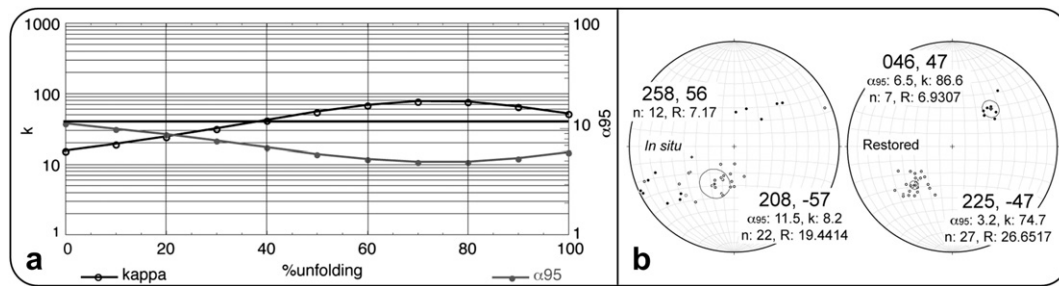
Fig. 5. a) Significant fold test at 70% (McElhinny, 1964 run under SuperIAPD) performed with high quality sites (α_{95} <10°). b) *In situ* (where α95 and k are absent for normal component) and *restored* projections also suggest a pre-folding magnetization.

progressively younger sediments placed in less oblique positions. The accurate chronological frame of rotation of structures and the exact amount of rotation (Fernández-Bellón, 2004; Mochales et al., 2008) are not solved yet, becoming key questions for the complete understanding of the kinematics of the South Pyrenean Zone.

5.1. Rotation magnitudes

Differences between declination angles and the Eocene reference are interpreted as VARs. Time-rotation relationships were established considering both all the dataset (Fig. 6a) and only the new data (Fig. 6b,c). After filtering (sample and site scales), individual sites still display variable magnitudes of clockwise rotations ranging between +63° and −3°, with +34° the total average (Fig. 6a). The entire rotation is bracketed within the Eocene (Ogg and Smith, 2004). It is worth noticing that the average is strongly influenced by a clear rotation-decreasing pattern during Bartonian-Priabonian times. Thus, we went one step further to obtain a robust time/rotation dataset (Pueyo et al., 2002) and we grouped the selected sites into nine, 2 m.y. age-sets (Fisher, 1953). The final goal was to obtain a trustworthy temporal evolution of the VARs (Fig. 6b) and the velocity and acceleration of the rotational process (Fig. 6c). This picture shows clockwise rotations ranging between +52° and non-significant, with a clear pattern of decreasing rotation values for younger sediments. An apparent relative 14 ° CCW rotation appears in the first age-set, with a maximum declination in Ilerdian-Cuisian rocks. However, in these sites the paleomagnetic vector is strongly influenced by the irregular signal of Alveoline limestones and Metils Fm (see Fig. 6).

Neglecting these first noisy data, the rotational evolution fits a logarithmic curve (R: 0.96) with a diversion that begins at around 42 M.a. This evinces a stable and decreasing trend from Ilerdian (rocks rotated +52°) to the Upper Lutetian (rocks rotated +37°, with 15° of CW VAR during this period), and an abrupt decay of rotation values in Upper Lutetian to Priabonian (non-rotated) rocks.

A logarithmic curve implies that the rotational velocity describes a hyperbolic behaviour and an acceleration of the movement linked to the emplacement of the SPCU thrust sheets. An interpretation can be done in these terms: the natural logarithmic function is a progressive curve that encompasses the whole Eocene epoch. This curve presents an initial CW rotation during the Ypresian and most part of the Lutetian. From about the Late Lutetian this trend changed, and accelerated around the Bartonian-Priabonian boundary, with a very strong rotation rate during the Priabonian, that definitively emplaced the Boltaña-Balzes anticline in its present-day orientation. Sites located in Middle Priabonian units record paleomagnetic vectors parallel to the reference direction and therefore indicate the end of the rotational motion. Assuming that the youngest age for the Boltaña folding is Late Bartonian (De Federico, 1981; Montes, 1992, Teixell, 1992, 1996), the Bartonian

rotation could be still related to the movement of the Boltaña-Balzes thrust sheet. However, at least the Priabonian rotation would be related to an underlying thrust sheet: most probably the Tozal-Alcanadre sheet (Millán, 1996). The Boltaña-Balzes sheet would be located in the hanging wall of this sheet, along a flat and a low-angle ramp (cross-section 2-2', Millán, 1996, Fig. 1). The absence of evidence of stepwise rotation precludes determining whether the rotational movements were distributed in both thrust sheets or linked only to the Tozal-Alcanadre thrust. This means that the Bartonian rotation would be contemporary with the uplift of the Boltaña anticline, whereas the subsequent stage merely implies rotational deformation. Once rotational movement ended, deformation migrated to the west, towards the External Sierras (Millán et al., 2000). Further studies in the lower thrust sheet should focus on this question.

5.2. Velocity model of thrust rotation

The available chronostratigraphy based on paleomagnetic data along the entire Ainsa Basin sequence (Mochales et al., 2011) allows us to propose a chronological frame for the rotation magnitudes. Considering the logarithmic fit and the α_{95} angles, moderate (non-significant) rotation took place during the approximate 56−42 M.a. interval (Ilerdian-Middle Lutetian). The rotation rate would accommodate 15° in 14 m.y. (average rotation rate 1.2°/m.y.), with practically constant velocity. The ages for establishing the change in trend have been selected from the derivatives with the aim of describing the rotation. This adjustment implies an increase in rotation velocity towards the end of this deformation period (42−35 M.a., Late Lutetian-Middle Priabonian), with an initial rotation rate of 2.6°/m.y. progressively increasing to reach 10°/m.y. in Priabonian times, to finally accommodate the finite rotation value of 37° (Fig. 6c). This last period would be characterised by variable angular acceleration around 1.5°/m.y.[2]. A period of strong acceleration during the Priabonian was followed by a well-anchored sharp end of rotation at 35 M.a. Therefore the final rotation of the Boltaña-Balzes/Tozal-Alcanadre thrust system occurred from Late Lutetian to Middle Priabonian (coinciding with the sedimentation of the whole Escanilla Fm). This sudden stop can be included within the context of clockwise rotations related to oblique structures linked to the emplacement of thrust units in the SPCU. Rotation in this area can be understood as a secondary process occurring at lateral termination of thrusts and therefore dependent on thrust sheet displacement and transfer of displacement from one thrust sheet to another. This is especially common in cover thrust sheets underlain by a thick detachment level, as is the case of the Southern Pyrenees.

A number of previous studies indicate clockwise rotations in the Ainsa Basin and the External Sierras (Fig. 7 and Table 1: Bentham, 1992; Dinarès, 1992; Parés and Dinarès, 1993; Pueyo, 2000;
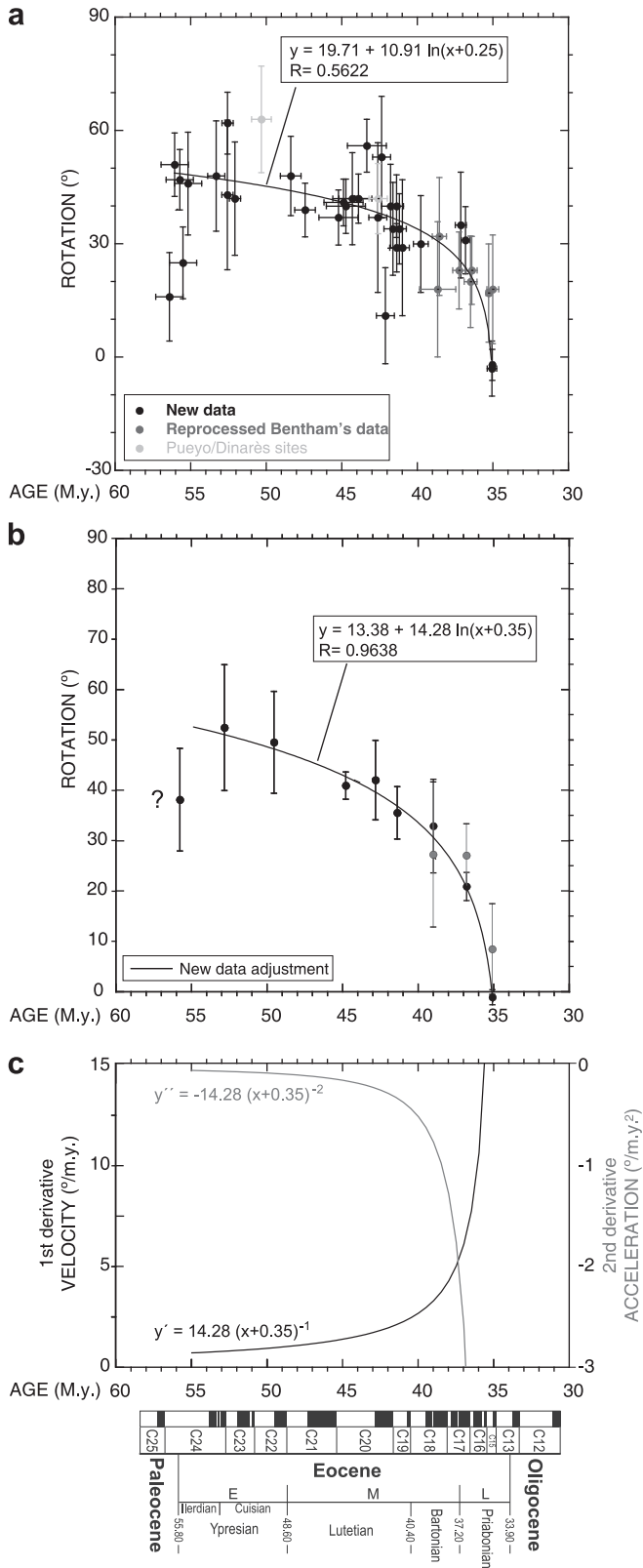
Fig. 6. Rotation vs. Age (time scale according to Gradstein et al., 2004) for the results obtained. a) Black points represent the data obtained in this work, dark gray, data reprocessed from Bentham's magnetostratigraphic profiles, and light gray represent sites studied by other authors (Dinarès 1992; Parés and Dinarès, 1993; Pueyo, 2000). In b and c, only the new data obtained in this work have been used, gathering them into nine set-ages. b) Rotational evolution can be approximated by a natural logarithmic equation whose detour occurs around at 42 M.a. c) First and second derivatives express the velocity and acceleration respectively, with a period of strong acceleration during Priabonian. In all logarithmic fits the time origin has been set out in 35 M.a.

Fernández-Bellón, 2004; Fernández et al., 2004). Fernández-Bellón (2004) proposed a regional 40–50° clockwise rotation in the Ainsa Basin, homogeneously accommodated from Early to Late Lutetian. In this paper, by means of accurate magnetostratigraphic dating of rotation, we propose a non-steady scenario with the main rotational movement younger than the one proposed by Pueyo et al. (1999) and Fernández-Bellón (2004). The rotation rate remains relatively stable from Ilerdian to Late Lutetian, with 15° in 14 m.y. Afterwards, a dramatic rotation of 37° occurred from Late Lutetian to Middle Priabonian times (6 m.y.), mainly developed during the Priabonian (see Table 1 and Figs. 6 and 7). This rotation explains the current N-S orientation of the Boltaña anticline, oblique to the WNW-ESE Pyrenean trend.

5.3. Paleocurrents and fold axis restoration

The results obtained allow for paleogeography of the Ainsa basin during the Eocene to be reconsidered. Taking into account paleomagnetic information, paleocurrents were restored to their original configuration before rotation of the Boltaña anticline. Compiled data include 70 directions from Van Lunsen (1970), 28 from Mutti et al.,(1985), 29 from De Federico (1981), and 43 from Barnolas et al. (in press-a, in press-b), considering bedding correction. Paleocurrents present S-N trends to the East of the Boltaña anticline, clearly defined in the south since they represent proximal areas of the continental margin, changing to NW trend in distal positions. To the west they show ESE-WNW trends.

After rotation restoration, considering the obtained rotation magnitudes, paleocurrents become ESE-WNW with scattering towards the SE (Fig. 8b) and better clustering. Therefore an ESE-WNW trough in the Buil syncline can be interpreted for the marine Eocene deposits. The Boltaña anticline would be nucleated, but not emerged, in Early Lutetian times (Mochales et al., 2010) permitting connection between sedimentation at its limbs during Early-Middle Lutetian times. During the Lutetian-Bartonian boundary, once rotational motion began, rocks located in the turbiditic trough were rotated. Paleocurrent directions (and perhaps the relative location of the source area) remained fairly constant (WNW-ESE) as witnessed by the directions indicated by the slightly rotated sediments of Bartonian age.

The axis of the Boltaña anticline can be restored in a similar way. Its present-day N004E trend (Mochales et al., 2010) has to be restored considering the bulk clockwise rotation (52°). Therefore a N128E orientation would be its original trend at the onset of deformation. In any case, this orientation would be associated with an oblique ramp, with the main trend of the Gavarnie-Larra thrust systems (E-W to WNW-ESE). The Boltaña anticline would be primarily nucleated oblique to the Pyrenean trend, as previously stated (Séguret, 1972). Several interpretations explain this obliquity as a consequence of thickening of the sedimentary pile (Soto and Casas, 2001; Soto et al., 2002), displacement gradients (Fernández-Bellón, 2004) or the push of previous oblique ramps towards the hinterland. Afterwards, obliquity was enhanced by Late Eocene rotation, where differential displacement of the thrust system must be invoked as the main reason for its kinematics.

5.4. Kinematic model

From the data obtained in this study a kinematic model can be proposed for the Boltaña anticline. Growth of the Boltaña anticline as an oblique ramp (N128E) began in the Early Lutetian. It gradually rotated 1.2°/m.y. on average during most of the Lutetian. From around the Late Lutetian the propagation of the deformation induced the movement of the Boltaña-Balzes sheet, recording the strong rotation during the Late Eocene. This pulse would take place
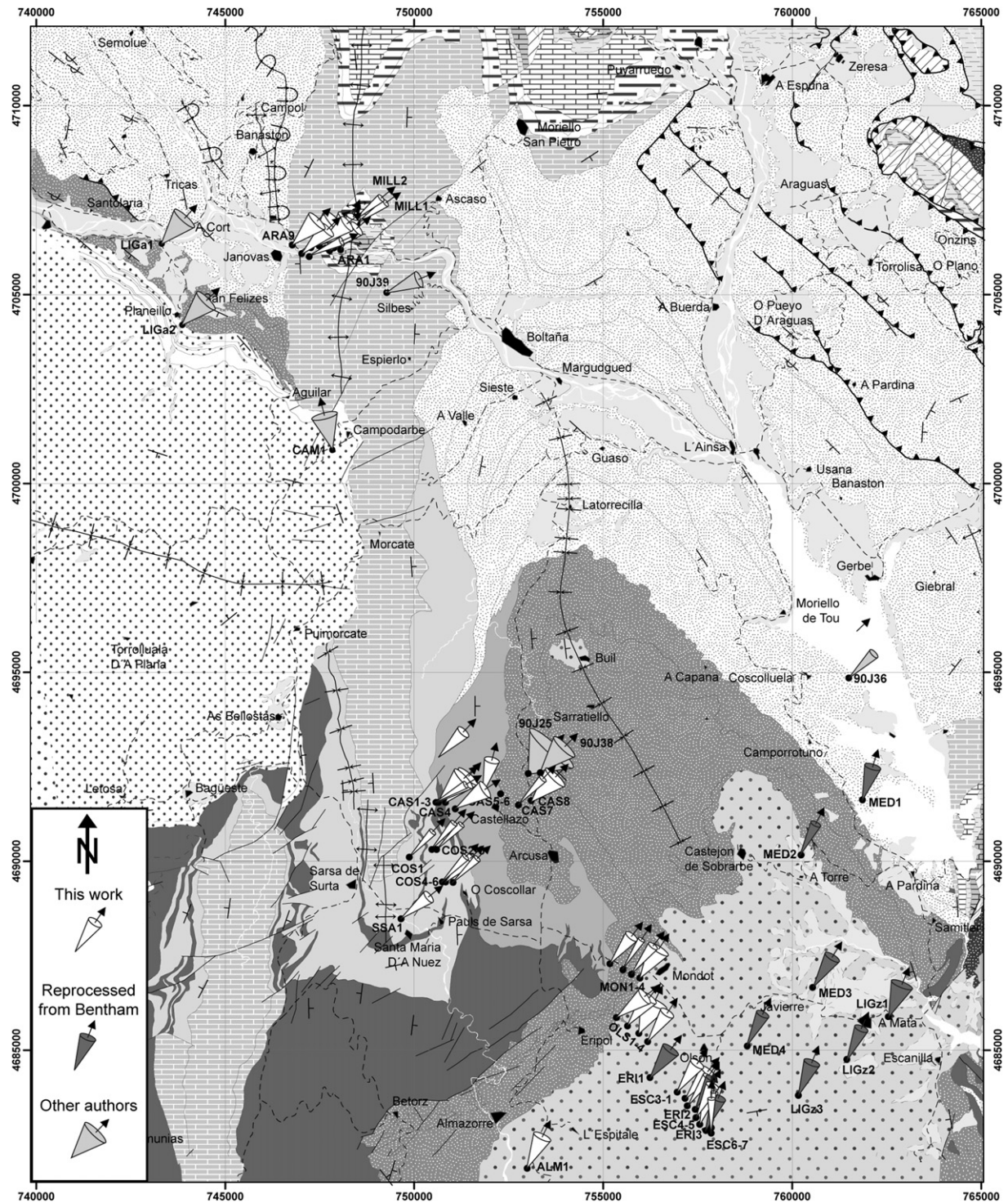
Fig. 7. Rotations in map view (axes of the cone represent the magnetic declination, semiapical angle of the cones is the α₉₅). White cones represent the data obtained in this work. Reprocessed Bentham's data are shown in dark grey. Data from Dinarès (1992), Parés and Dinarès (1993) and Pueyo (2000) are represented in light grey. Map modified form Barnolas et al. (in press-a, in press-b).

with an initial rotation velocity of 2.6°/m.y. (Late Lutetian-Late Bartonian) progressively increasing (10°/m.y. in Priabonian times). Complete cessation of the rotational movement occurred in the Middle Priabonian. During this time, the sedimentary scenario consisted of a fluvial network with meandering rivers flowing from SE to WNW (Escanilla and Campodarbe Fms, Fig. 9).

Assuming a length of 25 km for the Boltaña anticline and a 52° CW rotation, 21.9 km of oblique shortening must be accommodated

in its southern sector according to a simple model of map-view modelling of differences in shortening and rotations (Pueyo et al., 2004). Structures with NE-SW orientation, some of them showing a curved trace in map view (see geological map of Fig. 1 and Puigdefàbregas, 1975), could accommodate part, but not all of this movement. In contrast, considering a combined rotational and southward movement, the southward advance of the SPCU, displacing the Ainsa Basin and the Boltaña-Balzes and Tozal-Alcanadre
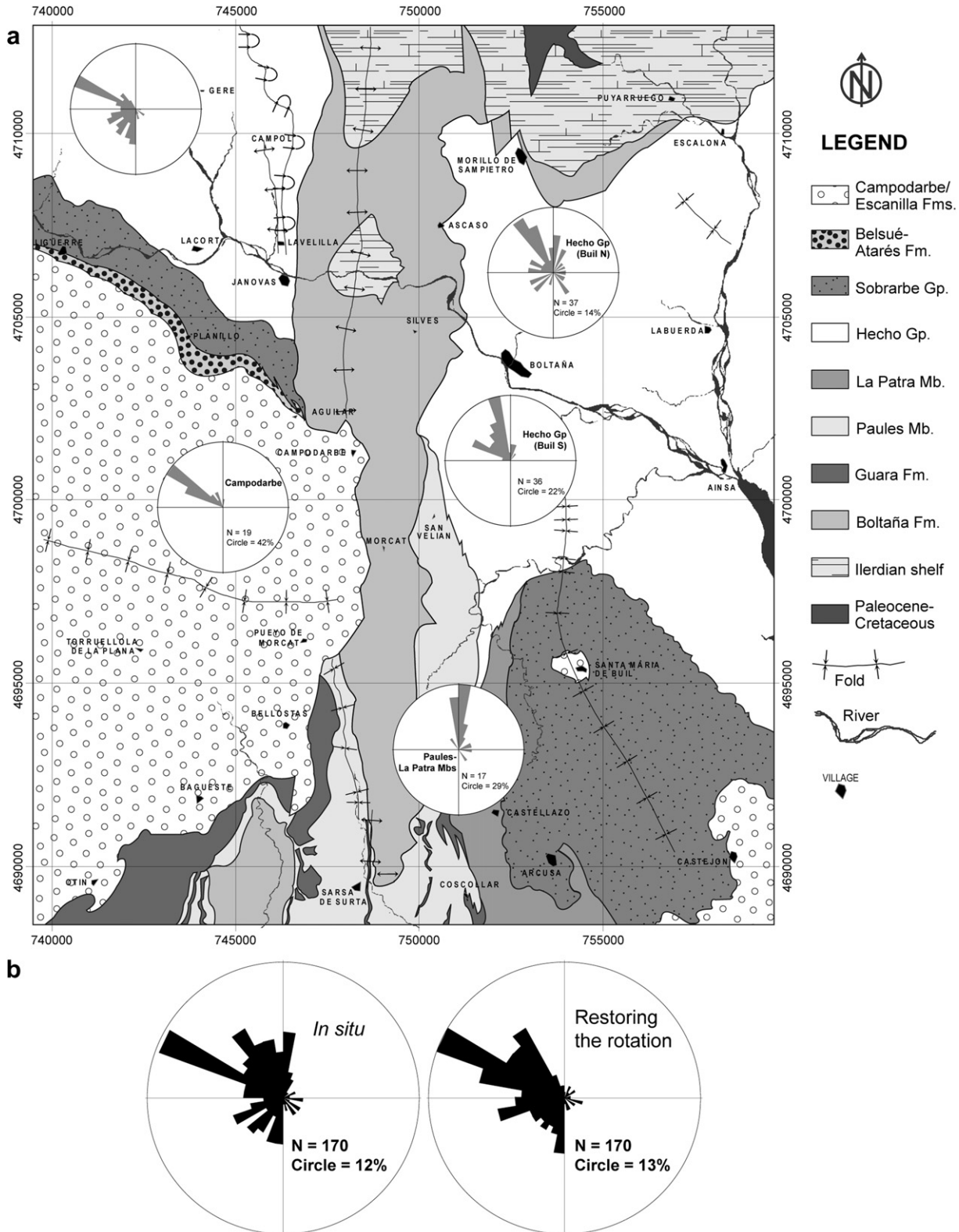
Fig. 8. a) Paleoflow data represented according to their lithostratigraphic position and geographic location, considering bedding restoration. Unit: Gp, Fm, Mb: Group, Formation, Member. b) Ensemble of paleoflow directions *in situ* (considering bedding) and restored according to the value of vertical axis rotation in each point. A better grouping is observed after rotation restoration.

sheets, would accommodate this differential displacement as a rotational transference.

Paleomagnetic analysis in equivalent rocks of the Mediano anticline, located immediately eastwards of the Boltaña anticline (Bentham's 1992 re-processed data), suggest that in that case folding and rotation were coeval. Nevertheless, the sites located in the western limb of the Mediano anticline (LIGz and MED) record lower declination angles than their equivalents located in the
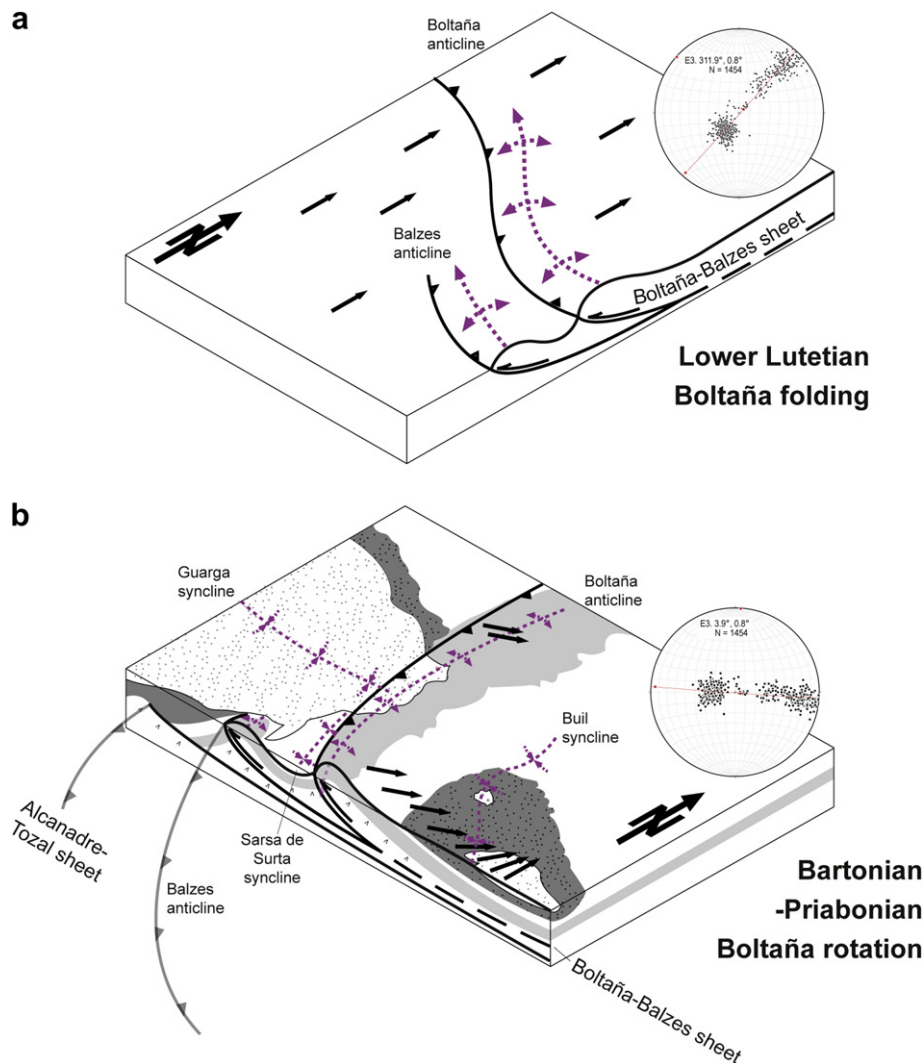
Fig. 9. Simplified sketches of the evolution of the western boundary of the SPCU with the magnetic declination from Lutetian to Priabonian. a) The Lutetian stage shows the Boltaña and Balzes anticlines with Pyrenean trend. Paleomagnetic vectors are parallel and N-directed during early diagenesis episodes. Equal area and E3 Bingham's distribution (1974) of bedding poles are shown (restored to their pre-rotational orientation). b) In the Bartonian-Priabonian stage rotational motion occurred below the Boltaña-Balzes sheet, due to the movement of the Alcanadre-Tozal thrust sheet, responsible for the passive rotation of the Boltaña-Balzes thrust sheet. Paleomagnetic vectors approach the magnetic north as rotation diminishes in younger sediments, dying out in Middle Priabonain. Equal area and minimum eigenvector of bedding poles are shown (field data).

eastern limb of the Boltaña anticline (ERI and ESC, Table 1 and Fig. 7). Consequently, the Mediano anticline rotated earlier than the Boltaña anticline, probably during Lutetian times (Poblet et al., 1998; Fernández-Bellón, 2004).

Since there are no structures able to accommodate differential shortening between the Boltaña and Balzes anticlines, located westwards, a rotational movement of the two structures, probably related to the rotational motion of an underlying and younger thrust sheet (Tozal-Alcanadre; Millán, 1996), must be invoked. A well-defined progressive unconformity within marine limestones denotes the onset of uplift of the Balzes anticline during the Lutetian-Bartonian transition (Barnolas and Gil-Peña, 2001; Rodríguez-Pintó et al., 2010). The Pico del Águila anticline, located westwards, underwent a quick CW rotation (7 to 10°/m.y.) in the Bartonian (Pueyo et al., 2002; Rodríguez-Pintó et al., 2008). The 30° rotation experienced by the Pico del Águila anticline was coeval and similar in magnitude to the first stage of rotation at the Boltaña anticline. Therefore the kinematic hypothesis of the west-wards migration of deformation in the External Sierras (Pueyo et al., 1999; Pueyo, 2000) can be refined with the results here obtained. Since the Boltaña and Balzes anticlines seem to rotate

synchronously, partly coinciding with rotation of the Pico del Águila anticline, a non-steady and more complex rotational deformation pattern can be proposed for the External Sierras basal thrust. The deformation would be effectively propagated west-wards during the emplacement of the SPCU; nevertheless this process is not continuous, showing a very slow rate during the Ypresian-Lutetian and a significant velocity during the Bartonian to Middle Priabonian episode.

6. Conclusions

From the continuous paleomagnetic record of Eocene rocks in the Boltaña anticline, the rotational evolution of this structure has been determined. Chronostratigraphy (Mochales et al., 2011) and previous data (Bentham, 1992; Dinarès, 1992; Pueyo, 2000; Fernández-Bellón, 2004) allow us to verify the reliability of data and to bracket the magnitude of the rotation within its chrono-logical frame.

Paleomagnetic data indicate a significant clockwise rotation of the structure, with a dramatic increase of rotation velocity during the Priabonian. This period with higher velocity would begin

during the deposition of the deltaic Sobrarbe Fm (circa 42 M.a.) to finally end at the top the Escanilla Fm. (35 M.a.). Early rotation velocities of 2.6°/m.y. can be assumed to follow a hyperbolic pattern, with maximum rates (10°/m.y) close to the end of the rotational process (Priabonian). The clockwise rotation here documented can be conceived as a secondary process related to oblique termination of thrust sheets undergoing differential displacement.

The rotation of the Boltaña anticline is probably linked to the movement of an underlying, younger thrust sheet (Tozal-Alcanadre) detached at the Upper Triassic evaporite levels. Boltaña-Balzes folding started in Early Lutetian stages with a NW-SE trend, and progressively acquired the present trend during the Eocene. Paleocurrent analyses indicate relatively constant NW-directed flow, with older (Lutetian-Bartonian) paleocurrent indicators rotated to a N–S orientation and the younger, non-rotated ones (Priabonian) retaining their original NW-SE orientation.

The results obtained in this work and comparison with previous results by other authors indicate that isolated sites must be carefully considered, and that it is necessary to acquire several sites in the same location with the aim of evaluating lithological and tectonic controls. To avoid these interferences, and to diminish noisy signal, homogeneous, dense and age-controlled datasets are recommended.

Acknowledgements

References

Allerton, S., 1998. Geometry and kinematics of vertical-axis rotations in fold and thrust belts. Tectonophysics 299 (1–3), 15–30.

Anastasio, D.J., 1992. Structural evolution of the External Sierra, Spanish Pyrenees. In: Mitra, S., Fisher, G.W. (Eds.), The Structural Geology of Fold and Thrust Belts. Johns Hopkins Univ. Press, Baltimore, Md, pp. 239–251.

Arriagada, C., Roperch, P., Mpodozis, C., Cobbold, P.R., 2008. Paleogene building of the Bolivian Orocline: tectonic restoration of the central Andes in 2-D map view. Tectonics 27. doi:10.1029/2008TC002269.

Barnolas, A., Samsó, J.M., Teixell, A., Tosquella, J., Zamorano, M., 1991. Evolución sedimentaria entre la cuenca de Graus-Tremp y la cuenca de Jaca-Pamplona. I Congreso del Grupo Español del Terciario, Libro-Guía de la excursión n° 1, EUMO Gràfic, Vic, 123 p.

Barnolas, A., Teixell, A., 1994. Platform sedimentation and collapse in a carbonate-dominated margin of a foreland basin (Jaca basin, Eocene, southern Pyrenees). Geology 22, 1107–1110.

Barnolas, A., Gil-Peña, I., 2001. Ejemplos de relleno sedimentario multiepisódico en una cuenca de antepaís fragmentada. La Cuenca Surpirenaica. Boletín Geológico y Minero 112 (3), 17–38.

Barnolas, A., Montes, M., Malagón, J., Gil-Peña, I., Rico, M., in press-a. Memoria y Hoja Geológica número 211 (Boltaña) del Mapa Geológico de España. Instituto Geológico y Minero de España (2 Serie Magna), escala 1:50.000.

Barnolas, A., Samsó J.M., Malagón, J., Gil-Peña, I., Montes, M., Rico, M., in press-b. Memoria y Hoja Geológica número 249 (Alquézar) del Mapa Geológico de España. Instituto Geológico y Minero de España (2 Serie Magna), escala 1:50.000.

Bentham, P.A., 1992. The tectono-stratigraphic development of the western oblique ramp of the south-central Pyrenean thrust system, Northern Spain. Ph.D. thesis, University of Southern California. 253 p.

Bentham, P., Burbank, D.W., 1996. Chronology of Eocene foreland basin evolution along the western oblique margin of the South-Central Pyrenees. In: Friend, P.F., Dabrio, C.J. (Eds.), Tertiary Basin of Spain. Cambridge University Press, Cambridge, UK, pp. 144–152.

Cámara, P., Klimowitz, J., 1985. Interpretación geodinámica de la vertiente centro-occidentalsurpirenaica(CuencasdeJaca-Tremp).Estudiosgeológicos41,391–404.

Choukroune, P., ECORS team, 1989. The ECORS Pyrenean deep seismic profile reflection data and the overall structure of an orogenic belt. Tectonics 8 (1), 23–39.

De Federico, A., 1981. La sedimentación de talud en el sector occidental de la cuenca paleógena de Aínsa. Ph.D. thesis, Publicaciones de Geología, Universitat de Barcelona, 12. 271 p.

Dinarès, J., 1992. Paleomagnetisme a les Unitats Sudpirinenques Superiors. Implicacions estructurals. Ph.D. thesis, Universtat de Barcelona, 462 p.

Farrell, S.G., Williams, G.D., Atkinson, C.D., 1987. Constraints on the age of movement of the Montsech and Cotiella thrusts, south central Pyrenees, Spain. Journal of the Geological Society London 144, 907–914.

Fernández-Bellón, O., 2004. Reconstruction of geological structures in 3D. An example from the Southern Pyrenees. Ph.D. thesis, Universitat de Barcelona. 321 p.

Fernández, O., Muñoz, J.A., Arbués, P., Falivene, O., Marzo, M., 2004. Three-dimensional reconstruction of geological surfaces: an example of growth strata and turbidite systems from the Ainsa Basin, Pyrenees, Spain. American Association of Petroleum Geologists Bulletin 88 (8), 1049–1068.

Fonnesu, F., 1984. Estratigrafía física y análisis de facies de la secuencia de Fígols entre el río Noguera Pallaresa e Iscles (prov. de Lerida y Huesca). Tesis doctoral, Univ. Autònoma de Barcelona, 317 p.

Fisher, R.A., 1953. Dispersion on a sphere. Proc. R. Soc. London Ser. A 217, 295–305.

Garrido-Megías, A., 1968. Sobre la estratigrafía de los conglomerados de Campanué (Santa Liestra) y formaciones superiores del Eoceno (extremo occidental de la cuenca Graus-Tremp, Pirineo Central, provincia de Huesca). Acta Geol. Hispánica 3 (2), 39–43.

Garrido-Megías, A., 1973. Estudio geológico y relación entre tectónica y sedimentación del secundario y terciario de la vertiente meridional pirenaica en su zona central. Ph.D. thesis, Universidad de Granada, 395 p.

Gradstein, F.M., Ogg, J.G., Smith, A.G., 2004. Chronostratigraphy: linking tiem and rock. A geologic Time Scale. Cambridge University Press, Cambridge, 589 p.

Holl, J.E., Anastasio, D.J., 1995. Kinematics around a large-scale oblique ramp, southern Pyrenees, Spain. Tectonics 14 (6), 1368–1379.

Lanaja, J.M., 1987. Contribución de la exploración petrolífera al conocimiento de la Geología de España. Inst.Geol.Mine.España Ed. 465 p., 17 maps.

Larrasoaña, J.C., 2000. Estudio magnetotectónico de la zona de transición entre el Pirineo central y occidental; implicaciones estruucturales y geodinámicas. Ph.D. thesis, Universidad de Zaragoza, 287 p.

Larrasoaña, J.C., Parés, J.M., Pueyo, E.L., 2003. Stable Eocene magnetization carried by magnetite and magnetic iron sulphides in marine marls (Pamplona-Arguis Formation, southern Pyrenees, N Spain). Studia Geophysica Geodetica 47, 237–254. doi:10.1023/A:1023770106613.

Lowrie, W., 1990. Identification of ferromagnetic minerals in a rock coercivity and unblocking temperature properties. Geophysical Research Letters 17, 159–162.

Luzón, A., 2005. Oligocene–Miocene alluvial sedimentation in the northern Ebro Basin, NE Spain: Tectonic control and palaeogeographical evolution. Sedimentary Geology 177, 19–39.

Martínez Peña, M.B. 1991. La estructura del límite occidental de la unidad surpirenaica central. Ph.D. thesis, Universidad de Zaragoza. 380 p.

Martínez-Peña, M.B., Casas-Sainz, A.M., 2003. Cretaceous-Tertiary tectonic inversion of the Cotiella Basin (Southern Pyrenees, Spain). International Journal of Earth Sciences (Geol. Rundsch.) 92, 99–113.

Mattei, M., Petrocelli, V., Lacava, D., Schiattarella, M., 2004. Geodynamic implications of Pleistocene ultra-rapid vertical-axis rotations in the Southern Apennine (Italy). Geology 32 (9), 789–792. doi:10.1130/G20552.1.

McCaig, A.M., McClelland, E., 1992. Palaeomagnetic techniques applied to thrust belts. In: McClay, K.R. (Ed.), Thrust Tectonics. Chapman and Hall Eds., London, pp. 209–216.

McClay, K., Muñoz, J.A., García-Senz, J., 2004. Extensional salt tectonics in a contractional orogen: A newly identified tectonic event in the Spanish Pyrenees. Geology 32, 737–740.

McElhinny, M.W., 1964. Statistical significance of the fold tests in Paleomagnetism. Geophysical Journal of the Royal Astronomical Society 8, 338–340.

Millán, H., 1996. Estructura y cinemática del frente de cabalgamiento surpirenaico en las Sierras Exteriores Aragonesas. Ph.D. thesis, Universidad de Zaragoza, 330 p.

Millán, H., Pueyo, E.L., Aurell, M., Luzón, A., Oliva, B., Martínez-Peña, M.B., Pocoví, A., 2000. Actividad tectónica registrada en los depósitos terciarios del frente meridional del Pirineo central. Rev. Soc. Geol. España 13 (2), 279–300.

Mochales, T., Pueyo, E.L., Casas, A.M., Barnolas, A., 2008. Cinemática rotacional del anticlinal del Boltaña (Pirineo Central) durante el Luteciense. Geotemas 10, 1179–1182.

Mochales, T., Pueyo, E.L., Casas, A.M., Barnolas, A., Oliva-Urcia, B., 2010. Anisotropic magnetic susceptibility record of the kinematics of the Boltaña Anticline (Southern Pyrenees). Journal of Geology 45, 562–581. doi:10.1002/gj.1207.

Mochales, T., Barnolas, A., Pueyo, E.L., Serra-Kiel, J., Casas, A.M., Samsó, J.M., Ramajo, J., Sanjuán, J., 2011. Chronostratigraphy of the Boltaña anticline and the Ainsa Basin (Southern Pyrenees). Geological Society of America Bulletin. doi:10.1130/B30418.1.

Montes, M.J., 1992. Sistemas deposicionales del Eoceno medio-Oligoceno del sinclinorio del rio Guarga (cuenca de Jaca, Pirineo central). III Congreso Geológico España Simposios 2, 150–160.

Muñoz, J.A., 1992. Evolution of a continental collision belt: ECORSPyrenees crustal balanced cross-section. In: McClay, K.R. (Ed.), Thrust Tectonics. Chapman and Hall Eds., London, pp. 235–246.

Muñoz, J.A., Arbués, P., Serra-Kiel, J., 1998. The Ainsa Basin and the Sobrarbe oblique thrust system: sedimentological and tectonic processes controlling slope and platform sequences deposited synchronously with a submarine emergent thrust system. In: Hevia, A.M., Soria, A.R. (Eds.), Field Trip Guide Book, pp. 213–223. 15th IAS Congress, Alicante (Spain).

Mutti, E., Séguret, M., Sgavetti, M., 1988. Sedimentation and deformation in the Tertiary sequences of the Southern Pyrenees. In: AAPG Mediteranean Basins Conference, Nice. Field Trip Guidebook, vol. 7, pp. 1–169.

Mutti, E., Remacha, E., Sgavetti, M., Rosell, J., Valloni, R., Zamorano, M., 1985. Stratigraphy and Facies Characteristics of the Eocene Hecho Group Turbidite Systems, South-Central Pyrenees. In: Excursion Guidebook of I.A.S. 6th. European Regional Meeting. Excursion, vol. 12, pp. 519–576.

Ogg, J.G., Smith, A.G., 2004. The geomagnetic polarity time scale. A geologic Time Scale. Cambridge University press, Cambridge, 589 p.

Oliva, B., Pueyo, E.L., 2007. Rotational basement kinematics deduced from remagnetized cover rocks (Internal Sierras, Southwestern Pyrenees). Tectonics 26, TC4014,. doi:10.1029/2006TC001955.

Oms, O., Babault, J., Dinarès-Turell, J., Rouby, D., Remacha, E., Eichenseer, H., Urreiztieta, M., Nalpas, T., 2006. Validación de modelos geológicos y magnetotectónica. Ejemplo en la Cuenca Surpirenaica Central. In: Calvo, M., Garcés, M., Gomes, C., Larrasoaña, J.C., Pueyo, E., Villalaín, J.J. (Eds.), MAGIBER I, Paleomagnetismo en la Península Ibérica. Universidad de Burgos, pp. 41–44.

Parés, J.M., Dinarès, J., 1993. Magnetic fabric in two sedimentary rock types from the Southern Pyrenees. J. Geomag. Geoelectr 45, 193–205.

Poblet, J., Muñoz, J.A., Travé, A., Serra-Kiel, J., 1998. Quantifying the kinematics of detachment folds using three-dimensional geometry: Application to the Mediano Anticline (Pyrenees, Spain). Geological Society of America Bulletin 110, 111–125.

Pocoví, A., 1978. Estudio geológico de las Sierras Marginales Catalanas (Prepirineo de Lérida). Ph.D. thesis, Universitat de Barcelona, 218 p.

Pueyo, E.L., 2000. Rotaciones paleomagnéticas en sistemas de pliegues y cabalgamientos. Tipos, causas, significado y aplicaciones (ejemplos del Pirineo Aragonés). Ph.D. thesis, Universidad de Zaragoza. 296 p.

Pueyo, E.L., 2010. Evaluating the paleomagnetic reliability in folds and thrust belt studies. In: Marcos, A., Poblet, J. (Eds.), Trabajos de Geologia, vol. 30, pp. 145–154 (1).

Pueyo, E.L., Millán, H., Pocoví, A., Parés, J.M., 1999. Cinemática rotacional del cabalgamiento basal surpirenaico en las Sierras Exteriores Aragonesas: Datos magnetotectónicos. Acta Geológica Hispánica 32 (3-4), 119–138.

Pueyo, E.L., Millán, H., Pocoví, A., 2002. Rotation velocity of a thrust: a paleomagnetic study in the External Sierras (Southern Pyrenees). Sedimentary Geology 146, 191–208. doi:10.1016/S0037-0738(01)00172-5.

Pueyo, E.L., Pocoví, A., Millán, H., Sussman, A., 2004. Map-view models for correcting and calculating shortening estimates in rotated thrust fronts using paleomagnetic data. In: Sussman, A.J., Weil, A.B. (Eds.), Orogenic Curvature: Integrating Paleomagnetic and Structural Analyses. Geological Society of America Special Paper, 383, pp. 57–71.

Puigdefàbregas, C., 1975. La sedimentación molásica en la cuenca de Jaca. Pirineos 104, 188.

Puigdefabregas, C., Muñoz, J.A., Marzo, M., 1986. Thrust belt development in the eastern Pyrenees and related depositional sequences in the southern foreland basin. In: Allen, P.A., Homewood, P. (Eds.), Foreland Basins, vol. 8. Sp. Publ., Blackwell, IAS, pp. 229–246.

Quirantes J., 1978. Estudio sedimentológico y estratigráfico del terciario continental de los Monegros. Ph.D. thesis, Institución Fernando el Católico (CSIC). 27, 207p.

Remacha, E., Fernández, L.P., 2003. High-resolution correlation patterns in the turbidite systems of the Hecho Group; south-central Pyrenees, Spain. In: Mutti, E., Steffens, G.S., Pirmez, C., Orlando, M., Roberts, D. (Eds.), Turbidites;

models and problems. Marine and Petroleum Geology, vol. 20, pp. 711–726 (6–8).

Rodríguez-Pintó, A., Pueyo, E.L., Pocoví, A., Barnolas, A., 2008. Cronología de la actividad rotacional en el sector central del frente de cabalgamiento de Sierras Exteriores (Pirineo Occidental). Geotemas 10, 1207–1210.

Rodríguez-Pintó, A., Ramón, M.J., Oliva-Urcia, B., Pueyo, E.L., Pocoví, A., 2010. Errors in paleomagnetism: Structural control on overlapped vectors, mathematical models. Physics of the Earth and Planetary Interiors 186, 11–22. doi:10.3166/ga.23.151-165.

Roure, F., Choukroune, P., Berastegui, X., Mufioz, J.A., Villien, A., Matheron, P., Bareyt, M., Séguret, M., Cámara, P., Deramond, J., 1989. ECORS deep seismic data and balanced cross-sections: geometric constraints on the evolution of the Pyrenees. Tectonics 8, 41–50.

Séguret, M., 1972. Étude tectonique des nappes et séries décollées de la partie centrale du versant sud des Pyrénées - Caractère synsedimentaire, rôle de la compresion et de la gravité. In: Série géologie structurale, vol. 2. Publications USTELA, Montpellier, 155 p.

Soto, R., Casas, A.M., 2001. Geometría y cinemática de las estructuras norte-sur de la cuenca de Ainsa. Revista de la Sociedad Geológica 14, 3–4.

Soto, R., Casas, A.M., Storti, F., Faccenna, C., 2002. Role of lateral thickness variations on the development of oblique structures at the western end of the South Pyrenean Central Unit. Tectonophysics 350, 215–235.

Soto, R., Mattei, M., Casas, A.M., 2003. Relationship between AMS and folding in an area of superimposed folding (Cotiella-Bòixols nappe, Southern Pyrenees). Geodinamica Acta 16, 171–185.

Soto, R., Casas-Sainz, A.M., Pueyo, E.L., 2006. Along-strike variation of orogenic wedges associated with vertical axis rotations. Journal of Geophysical Research (Solid Earth) 111 (B10), B10402–B10423.

Speranza, F., Maniscalco, R., Mattei, M., Di Stefano, A., Butler, R.W.H., Funiciello, R., 1999. Timing and magnitude of rotations in the frontal thrust systems of southwestern Sicily. Tectonics 18, 1178–1197.

Sussman, A.J., Butler, R.F., Dinarès-Turell, J., Vergés, J., 2004. Vertical-axis rotation of a foreland fold and implications for orogenic curvature: an example from the Southern Pyrenees, Spain. Earth and Planetary Science Letters 218, 435–449.

Taberner, C., Dinarés-Turell, J., Giménez, J., Docherty, C., 1999. Basin infill architecture and evolution from magnetostratigraphic crossbasin correlations in the southeastern Pyrenean foreland basin. Bulletin of the Geological Society of America 11, 1155–1174.

Teixell, A., 1992. Estructura alpina en la transversal de la terminación occidental de la zona axial pirenaica. PhD, thesis, Universitat de Barcelona, 252 p.

Teixell, A., 1996. The Ansó transect of the southern Pyrenees: basement and cover thrust geometries. Journal of the Geological Society 153, 301–310.

Teixell, A., 1998. Crustal structure and orogenic material budget in the west central Pyrenees. Tectonics 17 (3), 395–406.

Teixell, A., Muñoz, J.A., 2000. Evolución tectonosedimentaria del Pirineo meridional durante el Terciario: una síntesis basada en la transversal del río Noguera Ribagorçana. Revista de la Sociedad Geológica de España 13, 251–264.

Torsvik, T., 1986. Interactive Analysis of Palaeomagnetic Data: IAPD User-Guide. Universitetet i Bergen, 74 p.

Van der Voo, R., 1990. The reliability of paleomagnetic data. Tectonophysics 184, 1–9.

Van Lunsen, H., 1970. Geology of the Ara-Cinca region, Spanish Pyrenees. Province of Huesca. Ph.D. thesis, Utrech State University, Geol. Ultraiectina 16, 119 p.

Vergés, J., Muñoz, J.A., 1990. Thrust sequences in the Southern Central Pyrenees. Bulletin de la Société Géologique de France 8, 265–271.

Vergés, J., García Senz, J.M., 2001. Mesozoic Evolution and Cenozoic Inversion of the Pyrenean Rift. In: Ziegler, P.A., Cavazza, W., Robertson, A.H.F., Crasquin-Soleau, S. (Eds.), Peri-Tethys Memoir 6: Pery-Tethyan Rift/Wrench Basins and Passive Margins, vol. 186. Mémoires Muséum National d'Histoire Naturelle, pp. 187–212.

Weil, A.B., Sussman, A.J., 2004. Classification of curved ororgens based on the timing relationships between structural development and vertical-axis rotations. In: Sussman, A.J., Weil, A.B. (Eds.), Orogenic Curvature: Integrating Paleomagnetic and Structural Analyses, Spec. Pap. Geol. Soc. Am, vol. 383, pp. 1–17.

Weil, A.B., Yonkee, W.A., Sussman, A.J., 2010. Reconstructing the kinematics of thrust sheet rotation: a paleomagnetic study of Triassic redbeds from the Wyoming Salient, USA. Bulletin of the Geological Society Of America 122, 2–23.